

## THE IMPLANTATION AND INTERACTIONS OF $O^+$ IN TITAN'S ATMOSPHERE: LABORATORY MEASUREMENTS OF COLLISION-INDUCED DISSOCIATION OF $N_2$ AND MODELING OF POSITIVE ION FORMATION

M. B. SHAH<sup>1</sup>, C. J. LATIMER<sup>1</sup>, E. C. MONTENEGRO<sup>2</sup>, O. J. TUCKER<sup>3</sup>, R. E. JOHNSON<sup>3</sup>, AND H. T. SMITH<sup>4</sup>

<sup>1</sup> Department of Pure and Applied Physics, Queen's University Belfast, Belfast, UK

<sup>2</sup> Instituto de Física, Universidade Federal do Rio de Janeiro, Caixa Postal 68528, Rio de Janeiro 21945-970, RJ, Brazil

<sup>3</sup> Engineering Physics and Astronomy, University of Virginia, Thornton Hall B102, Charlottesville, VA 22904, USA

<sup>4</sup> Johns Hopkins Applied Physics Laboratory, Laurel, MD 20723, USA

Received 2009 April 9; accepted 2009 August 18; published 2009 September 15

### ABSTRACT

Energetic oxygen ions are an important component of the plasma incident onto Titan's atmosphere. Therefore, we report measurements of electron capture and ionization collisions of  $N_2$  with incident  $O^+$  over the energy range 10–100 keV. Using time of flight coincidence counting techniques we also measured the collision-induced dissociation of  $N_2$  following ionization and electron capture. The electron capture and ionization cross sections were found to have comparable magnitudes. Capture collisions are dominated by non-dissociative processes with the dissociative processes providing contributions that are only slightly smaller. In contrast, ionization is entirely dominated by the dissociative processes. The energy distributions of the  $N^+$  and  $N$  atom fragments ejected by 20, 50, and 100 keV incident  $O^+$  projectiles have also been determined. These fragments carry considerable amounts of energy and if produce in the exobase region can readily escape. The cross sections measured here have been used with Cassini energetic ion and atmospheric density data to determine the ionization by and neutralization of energetic  $O^+$  penetrating Titan's  $N_2$  rich atmosphere. Neutralization by charge exchange is found not to occur efficiently above Titan's exobase, so energetic particles with large gyroradii penetrate the atmosphere primarily as ions. When the energetic  $O^+$  flux is large, we also show it is an important source of ionization and heating at depth into Titan's atmosphere and the fragments contribute to the net atmospheric loss rate.

*Key words:* atomic processes – molecular processes – planets and satellites: individual (titan) – plasmas

### 1. INTRODUCTION

Titan, the largest moon of Saturn and the second largest moon in the solar system, has a substantial nitrogen atmosphere and is imbedded in an oxygen-rich plasma. Although its radius (2575 km) is about 40% of the Earth's radius, the atmospheric column density (number of molecules per unit area) is an order of magnitude larger than that at Earth. Like the Earth, Titan's atmosphere is dominated by molecular nitrogen, about 97%, with hydrogen, methane, and other hydrocarbons making up the rest (e.g., Niemann et al. 2005). This atmosphere has been suggested to resemble a primordial atmosphere on Earth, but it is unusually extended due to its much smaller gravity. That is, the exobase altitude, the altitude above which escape occurs and below which the atmosphere is collisional, is about 60% of the planet's radius (~1500 km) whereas at the Earth it is ~6%. Determining the origin and survival of this remarkable atmosphere has been one of the principal goals of the Cassini Mission.

Orbiting at a distance of  $20.6 R_s$  (Saturn radius ( $R_s$ ) ~ 60,268 km), which, under normal solar wind conditions, is inside the Saturn's magnetosphere, the major magnetospheric ions in the ambient plasma are  $H^+$ ,  $O^+$  with contributions from  $CH_x^+$  and  $N^+$  (Hartle et al. 2006). Because Titan does not have an intrinsic magnetic field, energetic ions from this plasma can penetrate its upper atmosphere (Ledvina et al. 2005; Sillanpaa et al. 2006, 2007; Ma et al. 2006).

Surprisingly, pre-Cassini observation (Coustenis et al. 1998) showed that in addition to hydrocarbons, *oxygen-containing molecules* were present in Titan's upper atmosphere a fact of interest to astrobiologists. Meteoroids were initially thought to be the source of oxygen, since the ambient plasma was

assumed to be dominated by  $H^+$  and  $N^+$  and the surface is extremely cold (~90 K) so that any water vapor is frozen out. However, based on data from the CAPS instrument (Cassini Plasma Science: Young et al. 2005), Hartle et al. (2006) showed that  $O^+$  is not only a principal heavy ion penetrating Titan's upper atmosphere, but the flux is sufficient to account for the required oxygen source rate. Since the ultimate sources of the  $O^+$  are the water geysers at south pole of Enceladus (Johnson et al. 2006a), with contributions from the oxygen atmosphere over Saturn's main rings (Johnson et al. 2006b) and sputtering of Saturn's E-ring particles (Johnson et al. 2008a), considerable transport is occurring in Saturn's magnetosphere (Johnson et al. 2005). Because of the importance of oxygen in the ambient plasma and the absence of cross section data for the energetic ions a series of measurements and modeling of the effect of keV  $O^+$  ions on  $N_2$  is described here.

The processes measured here, charge exchange and ionization with concomitant dissociations, are important when an  $O^+$  interacts with a neutral both in the extended regions of the atmosphere, called the atmospheric corona, and in the upper atmosphere, often called the thermosphere. Charge exchange of incident  $H^+$  and  $O^+$  produce energetic neutral atoms (ENA) that are unaffected by the local fields. The ENA produced in the corona not only directly penetrate Titan's upper atmosphere but are used by the Cassini spacecraft to image the corona (Garnier et al. 2007). In addition, in Luna et al. (2003) we showed that the energetic ions incident onto Titan's atmosphere contribute significantly to ionization to depths below the photoionization peak, and therefore, affects Titan's atmosphere at considerable depths. The incident ions also produce heating, collisional ejection of atoms and molecules (atmospheric sputtering), and expansion of the corona (e.g., Johnson 1994; Shematovich et al.

2003; Michael et al. 2005; Michael & Johnson 2005; Johnson 2009).

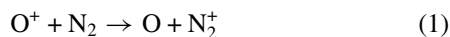
New ions produced by charge exchange and ionization in Titan's corona are accelerated by the local fields contributing to mass loading of Saturn's magnetosphere (e.g., Sillanpaa et al. 2007). These ions are either swept away contributing to loss of atmosphere (e.g., Wahlund et al. 2005; Hartle et al. 2006) or reimpact the atmosphere producing atmospheric sputtering (Johnson et al. 2009). Since Cassini data has confirmed that energetic  $O^+$  penetrates the exobase (Hartle et al. 2006) and  $N_2$  is the major species in Titan's upper atmosphere, high quality ion and electron impact cross sections with  $N_2$  as the target are needed.

In an earlier paper, we reported measurements of  $H^+$  and  $N^+$  projectiles colliding with  $N_2$  (Luna et al. 2003), of relevance to Titan's atmosphere, and of  $H^+$  and  $O^+$  projectiles colliding with  $O_2$  (Luna et al. 2005), of relevance to Europa's atmosphere. Using coincidence counting techniques, we showed that electronic interactions play a very significant role in the 10–100 keV energy range studied, resulting in very large cross sections for electron capture and target ionization. These interactions were shown to be accompanied by large amounts of molecular dissociation releasing fragments carrying sizable amounts of kinetic energy. Electronic processes are thus of paramount importance in the modeling of energetic ion–molecule collisions in planetary atmospheres.

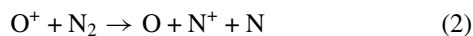
In this paper, cross sections for charge exchange and ionization of  $N_2$  by  $O^+$  are reported in order to supplement our earlier measurements for  $H^+$  and  $N^+$  incident on  $N_2$  (Luna et al. 2003). When Titan is within Saturn's magnetosphere, which is the case most of the time, the energy flux is primarily carried by the 10–100 keV ions. Whereas the  $H^+$  ions have the dominant energy flux in the ambient plasma, because of their large gyroradii the  $O^+$  ions appear to be dominating the plasma energy deposition rate into Titan's upper atmosphere (Hartle et al. 2006; Sillanpaa et al. 2007). Since heating and atmospheric escape at Titan also depend on the fragmentation produced, dissociation cross sections and fragment energy spectra are also measured.

## 2. CROSS SECTIONS

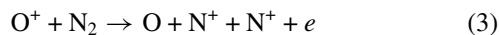
We have used time of flight (TOF) coincidence counting techniques to measure the individual dissociative and non-dissociative cross sections for  $N_2$  in collision with  $O^+$  ions over the 10–100 keV incident energy range. The measured capture cross sections were



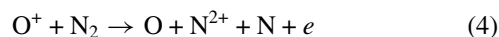
for the non-dissociative collisions leading to  $N_2^+$  formation,



for the dissociative collisions leading to  $N^+ + N$  formation,



for the dissociative transfer ionization (TI) collisions leading to  $N^+ + N^+$  pair formation, and



for the dissociative TI collisions leading to  $N^{2+}$  formation.

The ionization cross sections were also measured for the non-dissociative collisions

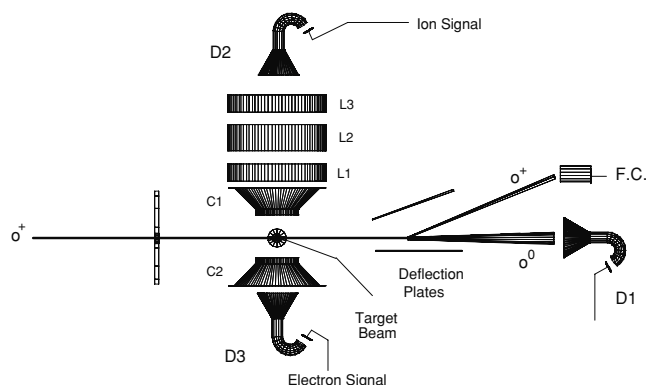
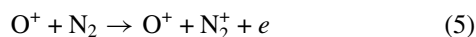
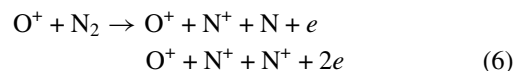
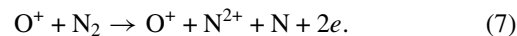


Figure 1. Schematic diagram of the apparatus.

leading to  $N_2^+$  formation, the total  $N^+$  ion production in the dissociative collisions



leading to  $N^+ + N$  and  $N^+ + N^+$  pair formation and the dissociative collisions



leading to  $N^{2+}$  formation.

Further collision channels involving projectile electron loss are possible, but these were not considered in the present investigation. Dissociative processes follow the formation of excited electronic repulsive states and produce target fragments with kinetic energies often large enough to escape from the planet atmosphere (e.g., Luna et al. 2003, 2005). Therefore, the energy spectra of these ejected fragments were also measured.

## 3. EXPERIMENT

The main apparatus and experimental procedure has been described previously (Luna et al. 2003; McCartney et al. 1999; McGrath et al. 2001) and only the main features and minor modification are summarized here. Figure 1 shows the schematic diagram of the apparatus used. A pulsed beam of  $O^+$  ions was crossed at  $90^\circ$  by a well-collimated thermal energy beam of  $N_2$  inside a high vacuum main chamber. Slow target ion and electron products were extracted from the interaction region in opposite directions to one another by electric field applied across cones C1 and C2 and were detected using channel electron multipliers D2 and D3, respectively. Lens L1, L2, and L3 were used to maximize the detection of all the extracted target ion products. The target ion products were distinguished from one another by the TOF of the ions to D2. The reaction channels (1) and (4) associated with electron capture were identified by recording the target ion products in coincidence with the fast neutral products detected by D1, as was the sum of channels (2) and (3). Channel (3) was uniquely determined by triple coincidences involving detectors D1, D2, and D3. The ionization channels (5), (6), and (7) were identified by recording the coincidences between the target ion products and the emitted target electrons (see Luna et al. 2003). The present cross sections have been normalized to the well-established total one electron capture cross sections of Stier & Barnett (1956) for proton impact which are believed to be accurate to within 5%. The  $O^+$  projectile beam was replaced with an  $H^+$  beam for this purpose.

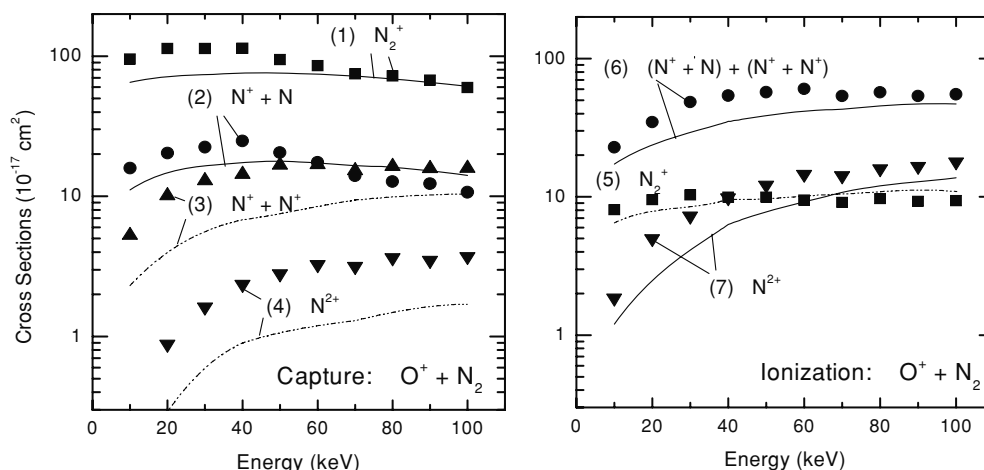


**Figure 2.** Dissociative and non-dissociative cross sections for O<sup>+</sup> impact on N<sub>2</sub> for one-electron capture (left panel) and target ionization (right panel). Our previously measured cross sections for N<sup>+</sup> impact (Luna et al. 2003) are shown, for comparison, as lines.

**Table 1**  
Cross Sections for the Dissociative and Non-dissociative Capture and Ionization Channels (1)–(7) in Units of 10<sup>-17</sup> cm<sup>2</sup> for O<sup>+</sup> Ion Impact on N<sub>2</sub>

E (keV)	Channel Number						
	(1)	(2)	(3)	(4)	(5)	(6)	(7)
10	95 ± 7	16 ± 2	5.3 ± 0.6	...	8.1 ± 1.1	23 ± 4	1.9 ± 0.3
20	113 ± 8	20 ± 2	10.1 ± 1.2	0.9 ± 0.2	9.5 ± 1.3	35 ± 6	5.0 ± 0.7
30	113 ± 8	22 ± 2	12.9 ± 1.4	1.6 ± 0.2	10.3 ± 1.5	48 ± 6	7.3 ± 0.9
40	114 ± 8	25 ± 2	14 ± 1	2.4 ± 0.3	9.9 ± 1.5	54 ± 7	10 ± 1
50	94 ± 7	21 ± 2	17 ± 2	2.8 ± 0.4	9.9 ± 1.5	57 ± 6	12 ± 1
60	86 ± 6	17 ± 1	17 ± 2	3.3 ± 0.4	9.4 ± 1.5	60 ± 7	15 ± 1
70	75 ± 5	14 ± 1	15 ± 2	3.2 ± 0.4	9.1 ± 1.4	54 ± 7	14 ± 1
80	72 ± 5	12.8 ± 0.9	16 ± 2	3.7 ± 0.5	9.7 ± 1.5	57 ± 7	16 ± 2
90	67 ± 5	12.3 ± 0.8	16 ± 2	3.5 ± 0.5	9.3 ± 1.4	54 ± 6	16 ± 2
100	60 ± 5	10.7 ± 0.7	16 ± 2	3.7 ± 0.5	9.4 ± 1.4	55 ± 7	18 ± 2

For the energy distribution measurements of the ejected fragment ions, all the voltages applied across the interaction region and the drift region were set to a zero value. The ejected ions consequently proceeded to the detector D2 in absence of any external fields that might cause changes to their velocities. A reference pulse obtained from the main projectile beam pulsar was used as a start pulse in the recording of the energy related TOF spectra of these ejected ions. The measured TOF spectra were converted into energy spectra using standard procedures (Auerbach 1988).

Finally, it should be noted that the O<sup>+</sup> ion beams used in this work were obtained from a discharge ion source and, therefore, consisted of an unknown mixture of O<sup>+</sup> (<sup>4</sup>S) ground state ions and O<sup>+</sup> (<sup>2</sup>D) and O<sup>+</sup> (<sup>2</sup>P) metastable ions. However, at the impact energies employed in these measurements (>10 keV), it has been shown that these metastable ions have a negligible effect on the observed cross sections (Lindsay et al. 1998).

## 4. RESULTS AND DISCUSSION

### 4.1. Cross Section Measurements and Normalization

Our measured cross sections for the channels (1)–(7) for O<sup>+</sup> incident ions in N<sub>2</sub> are tabulated in Table 1 for incident energies ranging from 10 to 100 keV. The individual error bars (1σ) given in the table include contributions from statistical uncertainties in the accumulated counts, uncertainties in the reproducibility of the measurements due to fluctuations in pressure and incident beam current measurements, uncertainties in the calibration of the detectors and where appropriate errors

involved in subtraction procedures adopted to extract data for the individual channels (for further details, see Luna et al. 2003). The cross sections are subject to a further uncertainty of 9% for channels (1)–(4) and 14% for the remainder, resulting from normalizing uncertainties associated with assigning absolute values to our cross sections (Luna et al. 2003). The individual cross sections are shown in Figure 2.

It is apparent from Figure 2 that for electron capture, the non-dissociative channel (1) is the largest and the dissociative channels (2) and (3) are about an order of magnitude smaller while the channel (4) is about two orders of magnitude smaller. In contrast, for ionization, dissociation dominates and channel (6) is the most important. Even the dissociative ionization channel (7), leading to N<sup>2+</sup> production, is larger than the non-dissociative channel (5) for collisions above 40 keV.

For comparison, our previously measured cross sections for incident N<sup>+</sup> are included in Figure 2. As seen the cross sections involving O<sup>+</sup> projectiles are larger than those for N<sup>+</sup> for the majority of the channels especially at the lowest energies. This is partly due to the fact that O<sup>+</sup> moves more slowly than N<sup>+</sup> for a given energy. More important is the fact that the binding energy of the outer shell electrons in N<sub>2</sub> and O are such that the electron exchange interaction during the collision is larger (e.g., Johnson 1990) especially at the lower collision energies. The larger cross sections means that at energies ≲80 keV, O<sup>+</sup> is, on average, neutralized at higher altitudes in Titan's atmosphere than N<sup>+</sup>.

Figure 3 shows cross sections for the total ion production for the dissociative and the non-dissociative channels. Based

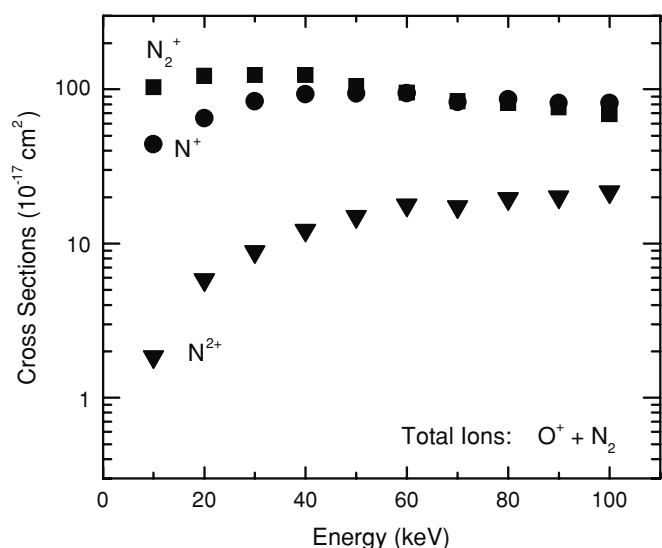


**Figure 3.** Cross sections for total ion production in both the dissociative and the non-dissociative channels for  $O^+$  projectiles in  $N_2$ .

on Figure 2, the majority of contributions to the dissociative  $N^+$  and the  $N^{2+}$  channels come from the ionization processes while those to the non-dissociative  $N_2^+$  channel come from the capture processes. For instance, the  $N^+$  channel receives 52% of the contributions from the ionization and 48% from the capture collisions at 10 keV becoming 67% and 33%, respectively, at 100 keV. For the  $N^{2+}$  channel, ionization and capture collisions contribute around 85% and 15%, respectively, over the energy range studied. For the non-dissociative  $N_2^+$  channel, the capture collisions contribute around 90% at all energies with ionization providing  $\sim 10\%$ . It is clear from Figure 3 that for total ion production, the dissociation collision process is as important as the non-dissociative collision process and becomes dominant at energies greater than 70 keV. The trends at low energy suggest that it will continue to remain a significant process below 10 keV.

#### 4.2. Fragment Energy Distributions

Dissociation is accompanied by a release of excess electronic energy in the form of kinetic energy carried away by the molecular fragments which contributes to the heating of upper atmosphere and to gravitational escape from Titan's atmosphere. The measurements of this kinetic energy release (KER) are also

of importance in understanding the fundamental atomic physics occurring as they contain vital information on the energy profiles of the populated repulsive states.

We have carried out the energy distribution measurements of the  $N^+$  ejected fragments by  $O^+$  projectiles at 20, 50, and 100 keV impact energies. Because  $N_2$  is a diatomic molecule, and dissociation is due to electronic excitations, the  $N$  fragments will have similar energy spectra. The KER spectra, shown in Figure 4, contain the contributions from both the capture and the ionization collisions and, as can be seen, the fragments are emitted with energies that extend well beyond a value of 20 eV. This should be compared to the energies required for the escape of  $N$  from Titan's exobase, the region of the upper atmosphere from which escape to space occurs with high probability ( $\sim 1450$  km above Titan's surface; Johnson et al. 2008b). A nitrogen atom produced during dissociation at the exobase requires only  $\sim 0.34$  eV to escape. This is close to the low energy limit of our KER spectra,  $\sim 0.3$  eV, so that most of the detected fragments have escape energies.

Our recent KER spectra for  $O^+$  incident on  $O_2$  (Luna et al. 2005) show the presence of many well-resolved peaks in the spectra. With the exception of the peak around 4 eV for 100 keV impact energy, the present spectra seem to contain only shallow bumps suggesting that, unlike in the case of  $O_2$ ,  $N_2$  fragmentation arises from a number of overlapping peaks corresponding to different reaction channels. We have used a least square fitting procedure to extract these peaks assuming that the individual profiles are Gaussians in shape. A comparison of the spectra around the 4 eV peak with the well-resolved spectra for  $O_2$  referred to above reveal that this assumption is justified. The extracted Gaussian peaks are shown in Figure 4 (as dashed curves) together with the total sum of all these peaks. As seen, the curve representing the sum reproduces the bumps in all of the three spectra remarkably well. This fitting procedure shows the presence of peaks appearing at the positions of 0.5 eV, 1.0 eV, 3.6 eV, 5.4 eV, 8.5 eV, and 14 eV. For the 20 keV incident energy, the 8.5 eV and 14 eV peaks were found to be small and are not included in Figure 4 for clarity.

The present KER spectra can be instructively interpreted with the aid of those of Yousif et al. (1990) and Lafosse et al. (2001) involving low energy  $He^+$  ion projectiles, the photoionization work of Nicolas et al. (2003), as well as the proton and electron impact studies of Ezell et al. (1984) and Lundqvist et al. (1996), respectively. The spectral features originate via the production of unstable precursor states of the  $N_2^+$  and  $N_2^{++}$  ions excited in

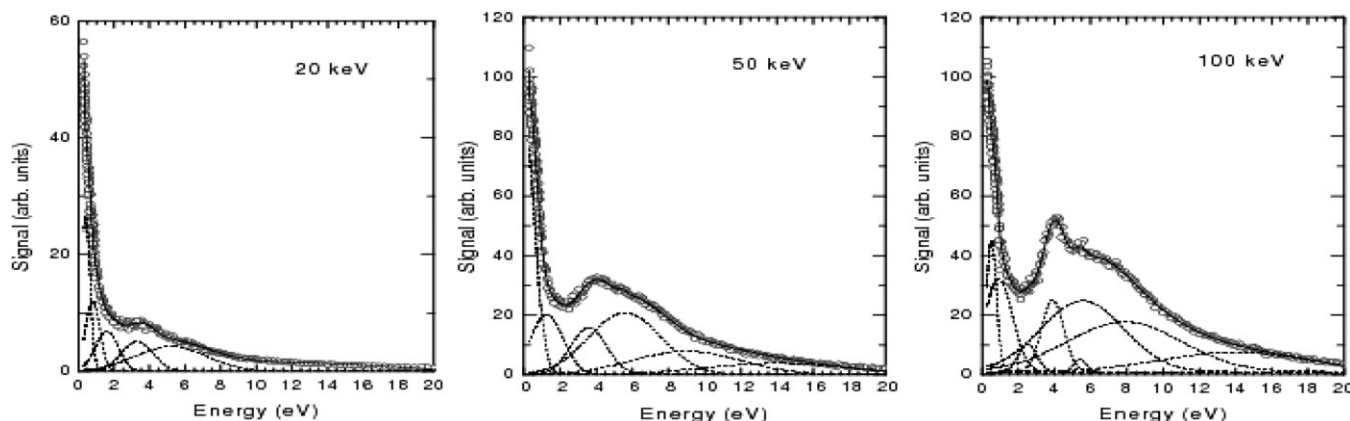


**Figure 4.** Kinetic energy distribution of the individual  $N^+$  fragments emitted at  $90^\circ$  to the  $O^+$  projectiles. Open circles represent the present data; dashed curves represent the Gaussian fits to the measured energy spectra and correspond to fragmentation arising from the precursor ion states of the  $O_2^{*+}$  and  $O_2^{++}$  (see the text); solid curve represents sum of all the dashed curves. Two highest energy dash curves for 20 keV are not shown for reasons of clarity.

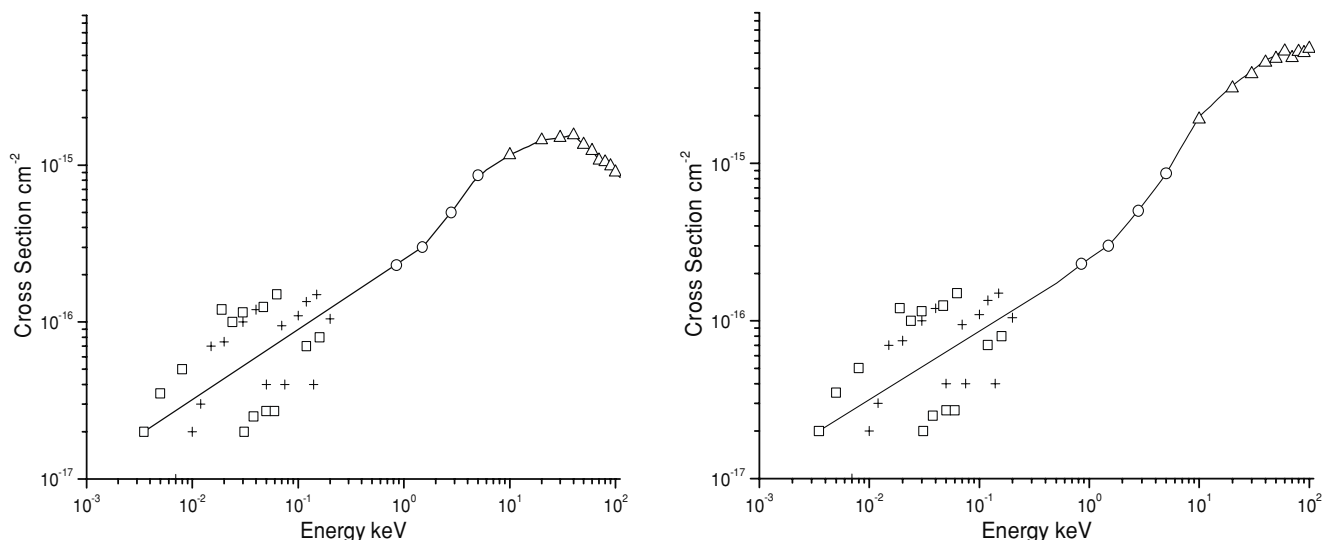


**Figure 5.** Summed cross sections vs. incident O<sup>+</sup> energy : (a) charge exchange (Equations (1)+(2)+(3)+(4)) and (b) net ionization produced (Equations (1)+(2)+(5)+(6)+2 × ((3)+(4)+(7))); crosses Flesch et al. (1990); squares Li et al. (1997); circles Lindsay et al. (1998); triangles (this work).

the Frank–Condon region, with the KER taken up by the N<sup>+</sup> ions identifying their energies in relation to their dissociation limit. Thus, from the known potential energy curves for N<sub>2</sub><sup>+</sup>, we can associate the two lowest energy peaks observed in the present work at 0.5 and 1.0 eV with excitation to the  $c^2\Sigma_u^+(v = 3-10)$  state of N<sub>2</sub><sup>+</sup>, which dissociates to form N<sup>+</sup>(<sup>3</sup>P) and N(<sup>4</sup>S) fragments, and the  $F^2\Sigma_g^+(v = v)$  state which dissociates to form N<sup>+</sup>(<sup>3</sup>P) and N(<sup>2</sup>D). The peaks at higher energies would appear to arise from Coulomb explosions of N<sub>2</sub><sup>++</sup> precursor ions to produce N<sup>+</sup> – N<sup>+</sup> ion pairs. They are, in general, substantially broader indicating that they arise from highly repulsive precursor states. It is interesting to note that a Coulomb explosion of the N<sup>+</sup> – N<sup>+</sup> system, starting from the equilibrium distance of the neutral N<sub>2</sub> molecule ( $r_e = 1.1 \text{ \AA}$ ) would result in fragment N<sup>+</sup> ions with an energy of 6.5 eV. Thus, the potential energy curves that are being populated lie both below and above the point charge Coulomb curve at the internuclear distance corresponding to the equilibrium separation between the two atoms in the N<sub>2</sub> molecule. The peak at 3.6 eV is a composite of excitation via the  $D^3\Pi_g$  and  $A^1\Pi_u$  states resulting in two N<sup>+</sup>(<sup>3</sup>P) ions and the 5.4 eV peak arises from the  $D^1\Sigma_u^+$  state producing N<sup>+</sup>(<sup>3</sup>P) and N<sup>+</sup>(<sup>1</sup>D) fragment ions. The identification of the higher energy states involved above the Coulomb curve, producing 8.5 and 14.0 eV fragment ions, is not certain and the increase in the width of the KER is connected with the spread of the potential energy curves being partly due to the mutual polarization of the fragments (Siegmann et al. 2000). The role and relative importance of these ion pair production processes increases substantially with increasing O<sup>+</sup> ion impact energy contributing about 28% at 20 keV and 43% at 100 keV.

## 5. TITAN'S ATMOSPHERE

The cross sections given in Table 1 provide details of the dissociative and non-dissociative ionization and charge exchange collisions produced by energetic O<sup>+</sup> that impact and penetrate Titan's predominantly nitrogen atmosphere. Total cross sections, cross sections for dissociation, and fragment energy spectra have been given. Previous low energy measurements of O<sup>+</sup> on N<sub>2</sub> have also shown that fragmentation is a *probable* outcome in ionization and charge exchange collisions (Flesch et al. 1990; Li et al. 1997), contrary to the statement in Cravens et al. (2008).

In Figures 5(a) and (b), we show the total charge exchange cross section (production of O ENAs) and the total ionization (production of total target charge) versus incident ion energy. It is seen that although the previous measurements are at much lower energies they exhibit trends which are consistent with our results. Using the cross sections in these figures and tables it is possible to model the effects produced in Titan's atmosphere by incident O<sup>+</sup> for energies <100 keV.

Since Titan has a highly extended atmosphere and no intrinsic magnetic field, the magnetospheric O<sup>+</sup> ions can penetrate the exobase causing heating of the thermosphere and ejection of atoms and molecules (Johnson 2009). In the energy range studied here (10–100 keV), the O<sup>+</sup> penetrate on an average a column  $\lesssim 2 \times 10^{18} \text{ N}_2 \text{ cm}^{-2}$ . Although this is a very small fraction of the total atmospheric column ( $\lesssim 2.5 \times 10^{26} \text{ N}_2 \text{ cm}^{-2}$ ), it is the region from which escape and photoionization occur, and it is also the region that is strongly affected by the interaction with Saturn's magnetosphere (Johnson et al. 2009). Although the surface temperature is estimated as 94 K, the temperature at the exobase is  $\sim 155 \text{ K}$ . This temperature slightly depends on the heating produced by the incident ions (Michael and Johnson 2005), which also collisionally eject atmospheric molecules (Michael et al. 2005). As stated earlier, the ions around mass 14–16 incident on Titan were initially thought to be N<sup>+</sup> but are actually O<sup>+</sup>. Therefore, the fraction of those energetic O<sup>+</sup> and their ENAs penetrating the exobase ( $\sim 0.5 \times 10^{15} \text{ N}_2 \text{ cm}^{-2}$ ) is of interest. If the scale of the ion's gyromotion is comparable to the radius of the obstacle, the ions are not efficiently deflected by the induced fields and penetrate into Titan's atmosphere. For the energy range considered here, the gyroradii for O<sup>+</sup> are of the order of  $\sim 4-12$  Titan radii when Saturn's magnetosphere is not significantly compressed by high solar activity. Therefore, Ledvina et al. (2005) and Sillanpaa et al. (2007) show that deflections of the ambient flux due to the induced fields are not sufficient to shield Titan from the energetic O<sup>+</sup> flux. These ions will, therefore, penetrate into and heat the upper atmosphere. However, the induced fields are sufficient to redirect the flow, so that the heating is non-uniform, a fact that will be considered in future modeling.

Here, we use an upper atmosphere model based on recent data from the Ion Neutral Mass Spectrometer (INMS) on the Cassini spacecraft (Magee et al. 2009). The atmospheric density versus

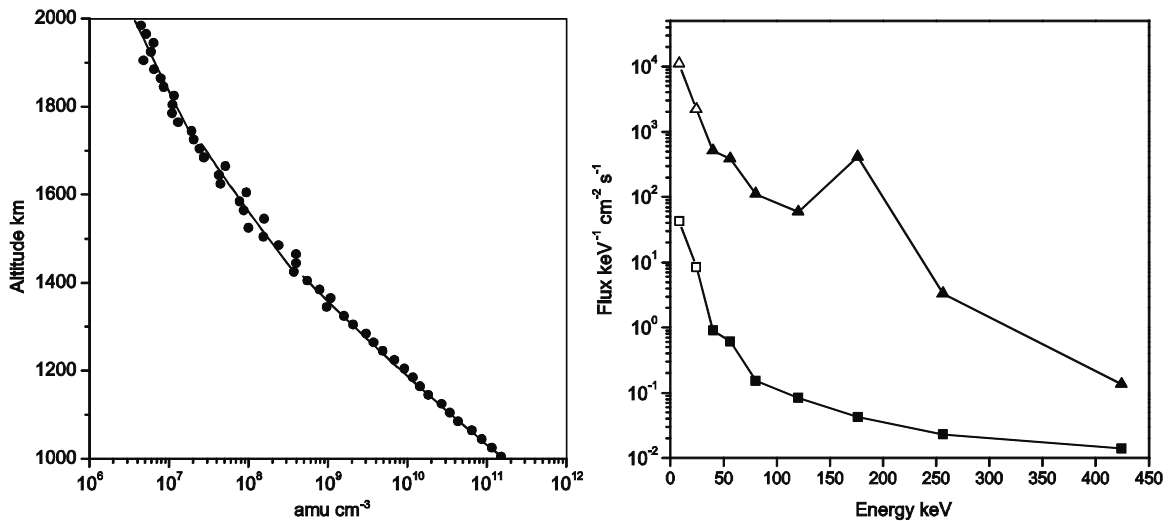


**Figure 6.** (a) Mass density vs. altitude above the surface of Titan's atmosphere. This is the average of a large number of passes through Titan's atmosphere as measured by the INMS instrument (e.g., De La Haye et al. 2007; Magee et al. 2009). Here we presume, for the estimates that follow, that the mass is all  $N_2$ , although with increasing altitude  $CH_4$  and  $H_2$  become a larger fraction of the total mass. Lines are rough exponential fits: scale heights 64, 101, and 198 km for the lowest middle and highest altitudes. (b)  $O^+$  flux ( $cm^{-2} s^{-1} keV^{-1}$ ) in energy bins detected by the INCA camera on the MIMI instrument on Cassini. The flux in the outer magnetosphere is highly variable due to a weak magnetic barrier being compressed by the variable solar wind. Shown are the largest flux ( $\times$ ) and a median (triangles) for a number of passes. Marks are centers of each energy channel with open marks extrapolated using a power law to the lowest E for which cross section was measured here. Net energy flux: median data:  $1.3 \times 10^7 eV cm^{-2} s^{-1}$ ; maximum data:  $8.3 \times 10^9 eV cm^{-2} s^{-1}$ .

altitude is given in Figure 6(a) and the  $O^+$  ion energies in the keV region, as measured by the MIMI Ion Neutral Camera (INCA) instrument on Cassini, are given in Figure 6(b). It is seen that the  $O^+$  flux is highly variable, depending on Titan's position in orbit and the configuration of Saturn's magnetosphere (Sittler et al. 2009; Rymer et al. 2009). For the range of ion energies studied here we give in Figure 7 the fraction of the incident  $O^+$  that are not neutralized versus depth into Titan's atmosphere assuming a predominantly nitrogen atmosphere. Based on the cross sections in Figure 5 about 10% of the 10–100 keV,  $O^+$  ions are neutralized before reaching the nominal exobase ( $\sim 1450$  km). The remainder of the ions penetrate the exobase and are subject to the local fields. In the absence of deflection by the fields or scattering, most of the  $\sim 10$ –100 keV  $O^+$  are neutralized by an altitude  $\sim 1200$  km above the surface and, therefore, deposit the remainder of their energy as energetic neutrals similar to the dominant incident proton flux (Smith et al. 2009).

The plasma flow inside Saturn's magnetosphere at Titan's radius is highly variable as is evident from the data in Figure 6(b). Models based on *Voyager* and Cassini data suggest the plasma  $O^+$  have a mean flow energy of  $\sim 1.2$  keV with a thermal distribution having a mean energy about twice of that. However, the ambient  $O^+$  flux has an extended tail in the energy range studied here (Dialynas et al. 2008). Whereas the total ambient energy flux for the ions is dominated by  $H^+$ , the models of the (Sillanpaa et al. 2007) have shown that the energetic  $O^+$  ions are the dominant source of energy for the upper atmosphere. The  $O^+$  flux in one set of simulations is  $\sim 1.3 O^+ cm^{-2} s^{-1}$  depositing  $\sim 310$  MW ( $\sim 2 \times 10^{27} eV s^{-1}$ ) which spread over an exobase area  $\sim 2 \times 10^{18} cm^2$  and gives a globally averaged plasma ion energy flux of  $\sim 1 \times 10^9 eV cm^{-2} s^{-1}$ . This is of the order of Cassini measurements of the ambient  $O^+$  fluxes penetrating the upper atmosphere (Hartle et al. 2006). It is also well within the range measured by the MIMI instrument on Cassini (e.g., Dialynas et al. 2008) as given in the caption for Figure 6 ( $(0.01$ – $8) \times 10^9 eV cm^{-2} s^{-1}$ ). Both the simulations and the measurements indicate that the plasma pressure varies considerably. When the

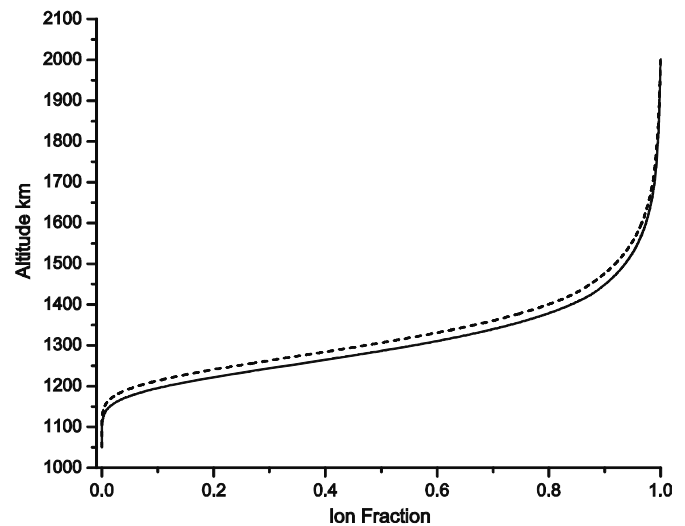


**Figure 7.** Fraction of incident 10 (dotted line) and 100 (solid line) keV  $O^+$  that are not neutralized as a function of altitude above the surface of Titan calculated using charge exchange cross sections in Figure 5(a) and the  $N_2$  density profile in Figure 6(a). The nominal exobase for escape of  $N_2$  is about 1450 km (the altitude above which collisions between atmospheric molecules become improbable and escape can occur). It is seen that the  $O^+$  remains substantially ionized well below the nominal exobase ( $\sim 1450$  km).

plasma pressure is large, the ambient heavy ions deposit a large amount of energy in the upper atmosphere.

Earlier we showed that the ionization produced by incident energetic protons was comparable to the photoionization (Luna et al. 2005). This ionization source is now thought to dominate deep into Titan's atmosphere (e.g., Cravens et al. 2008: the penetration calculation in this paper is questionable). Therefore, here we use a Monte Carlo particle tracking code to calculate the ionization contribution from the incident  $O^+$  ions. Since the cross sections discussed above go only to 100 keV, we consider the flux between 10 and 100 keV, use the atmospheric density in Figure 6(a) assuming it is all  $N_2$  and account for the loss

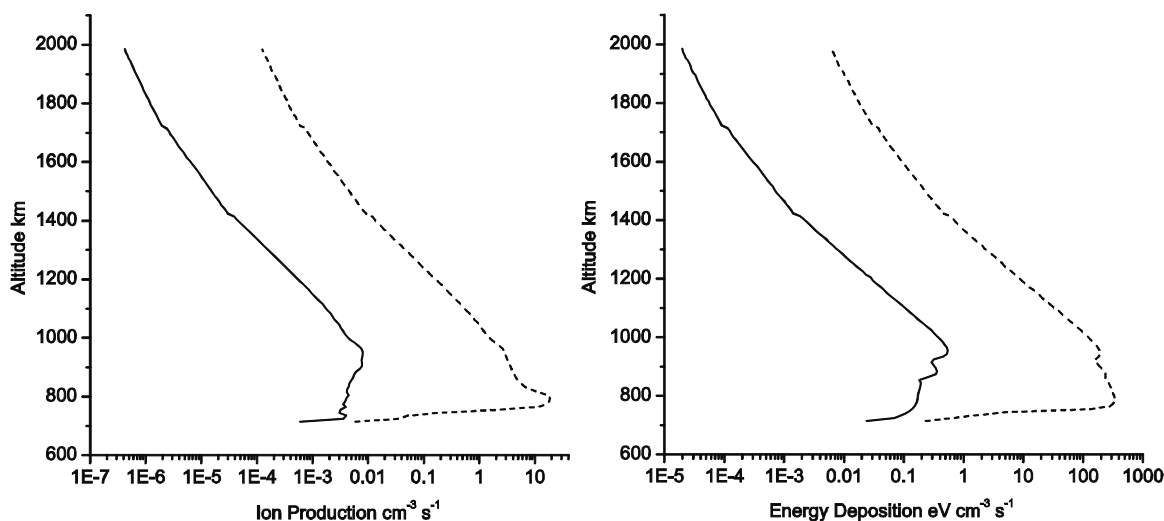


**Figure 8.** (a) Ionization rate ( $\text{cm}^{-3} \text{s}^{-1}$ ) and (b) energy deposition rate ( $\text{eV cm}^{-3} \text{s}^{-1}$ ) obtained using the energy spectrum in Figure 6(b) only between 10 and 100 keV and a cosine distribution starting altitude 2000 km above the surface; maximum (dashed) and median (solid). For the initial altitude and the angular distribution chosen for the incident ions,  $\sim 20\%$  of the incident energy flux is carried away by those ions with relatively large angles to the normal that leave the atmosphere, often as energetic neutrals.

of energy using the stopping cross section from Ziegler et al. (1985). We include the energy loss to both electronic excitations and ionization as well as to momentum transfer collisions which lead to deflections. Unlike in Cravens et al. (2008) where all the ions were assumed to enter normal to the exobase, here the flux was assumed to impact the atmosphere locally with a cosine distribution. The penetrating flux is multiplied by the  $\text{N}_2$  density and by the cross sections for ionization and charge exchange in Figures 5(a) and (b). In this manner, we give the ionization versus depth produced by the energetic  $\text{O}^+$  component of the plasma in Figure 8(a). This is shown for the largest flux among the samples analyzed and the median. In addition, we calculated the energy deposition per unit volume. In this case, we consider the ions with energies up to the maximum in Figure 6(b) and used the equilibrium charge state energy loss cross sections from Ziegler et al. (1985) for the combined  $\text{O}^+$  and  $\text{O}$  ENA flux. The equilibrium energy deposition versus depth into the atmosphere is shown in Figure 8(b). In both cases, we have not included the considerable contribution from the  $\text{O}^+$  ions with initial energies less than 10 keV (e.g., Hartle et al. 2006).

It is seen that the energy deposition and ionization rate can vary enormously depending on the plasma pressure. Although these globally averaged ionization rates for the median conditions in the measurement set are relatively small, the rates for the largest flux examined *exceed* those estimated earlier due to the protons (Luna et al. 2003; Cravens et al. 2008) even with the limited range of energies considered. Therefore, these ions can at times contribute significantly to the ionization at depth into Titan's atmosphere. In addition, when the plasma pressure corresponds to the largest flux presented here, the  $\text{O}^+$  ions are an important source of energy at depth into Titan's atmosphere.

The energy deposited by the incident  $\text{O}^+$  also produces escape, a process called atmospheric sputtering. This occurs primarily by momentum transfer collisions between the incident heavy ion and a neutral in the atmosphere (Michael et al. 2005). However, we showed here that ionization and charge exchange lead, with high probability, to dissociation with the fragments mostly having larger energies than the escape energy for an N atom ( $\sim 0.3$  eV). The resulting 'hot' fragments can escape directly, if produced within a scale height of the exobase, or they can collide and eject other atmospheric neutrals. Detailed modeling

is in progress using these measurements and extrapolations. However, the dissociation cross sections and the energy spectra can be used to estimate the direct escape of a fragment produced by ionization and charge exchange. Taking the sum of fragment cross sections and dividing by the total ionization produced, the number of fragments ( $\text{N}, \text{N}^+, \text{N}^{+2}$ ) per ionization goes from  $\sim 0.6$  to  $\sim 1$  as the energy goes from 10 to 100 keV. These fragments primarily have energies large than the escape energy, as indicated in Figure 4. Assuming, on average, one of the two fragments is directed outward, then the integrated ionization rate above the mean escape depth (Johnson 2009) gives a loss rate of  $\sim 10^5 \text{ N cm}^{-2} \text{ s}^{-1}$  for the larger ion flux. In addition, scaling the energy deposited in recoils to the simulations in Michael & Johnson (2005), a comparable mass flux of  $\text{N}_2$  is ejected by the recoils. The net is small compared to some recent estimates of the escape flux but those results are uncertain (e.g., Johnson et al. 2009). This estimate is a lower limit to the component produced by ionization-induced dissociation, since it includes only the ions in the energy range 10–100 keV.

## 6. CONCLUSIONS

We have carried out new measurements of the interaction of 10–100 keV  $\text{O}^+$  ions with  $\text{N}_2$  and report cross sections for ionization and charge exchange both with and without fragmentation of the target molecule. At our lowest  $\text{O}^+$  incident energies,  $\text{N}_2^+$  is the dominant product along with a significant level of fragmentation, while at our highest energies fragmentation dominates. In going from 10 to 100 keV, the fragment production rate varies from  $\sim 0.6$  to  $\sim 1$  per ion produced by ionization or charge exchange. The measured cross sections for incident  $\text{O}^+$  are found to be comparable to our earlier measurements for incident  $\text{N}^+$  ions at our highest collision energies but much larger than the  $\text{N}^+$  results at our lowest collision energies. It is also seen here that multiple ionization becomes a significant process at the highest collision energies. We have also presented energy spectra of the ejected fragments and show that substantial number carry ample energy to escape Titan's gravity if they are formed near the exobase. The recoils from dissociation also produce sputtering and heat the atmosphere (Johnson 1994).

In the energy range of interest (10–100 keV), the gyroradii of  $O^+$  are much larger than Titan's radius, so that the ions can penetrate Titan's atmosphere (Sillanpaa et al. 2007). Because Titan orbits in the outer regions of Saturn's magnetosphere, the heavy ion flux at Titan's orbital position in Saturn's equatorial plane can vary considerably as seen by the data in Figure 6(b). As shown here, at times this flux is an important, even dominant heat source at depth complimenting our earlier work on the incident proton flux (Luna et al. 2003; Smith et al. 2009). Therefore, the measured cross section data are now being used in simulations to describe the effect of the heavy ion plasma on atmospheric escape, ionization, and heating. Preliminary results are presented here for ionization, heating, and direct escape. Based on our measured cross sections, neutralization of the incident ions by charge exchange does not occur efficiently above the nominal exobase  $\sim 1450$  km. Therefore, the upper thermosphere is penetrated by energetic  $O^+$  ions. When the flux of  $O^+$  ions with energies less than 10 keV is included, the incident plasma can be the dominant source of energy near the exobase. The energy deposited by these ions in Titan's upper atmosphere acts to expand the upper atmosphere (Michael & Johnson 2005). This in turn increases the non-thermal escape rates and populates Saturn's plasma torus. For the largest flux shown here,  $O^+$  is an important ionization source at depth and may be the dominant external heat source for the upper atmosphere.

The authors thank D. G. Mitchell, the Cassini MIMI Instrument Scientist on Cassini, for access to and advice on the plasma data, J. Bell, J. Westlake, and B. Magee for access to and advice on their Cassini INMS data in advance of publication. E.M.C. acknowledges financial support from the Brazilian agencies CNPq and FAPERJ. M.B.S. and C.J.L. acknowledge financial assistance from the UK EPSRC. The work at Virginia was supported by NASA's Planetary Atmospheres Program.

## REFERENCES

- Auerbach, J. 1988, in *Atomic and Molecular Beam Methods*, Vol. 1, ed. G. Scoles (Oxford: Oxford Univ. Press), 365
- Bell, J. M., Bougher, S. W., Waite, J. H., Jr., Ridley, A. J., Magee, B., Bar-Nun, A., Toth, G., & De La Haye, V. 2009, *Planet. Space Sci.*, in press
- Coustenis, A., et al. 1998, *A&A*, **336**, L85
- Cravens, T. E., Robertson, I. P., Ledvina, S. A., Mitchell, D., Krimigis, S. M., & Waite, J. H. 2008, *Geophys. Res. Lett.*, **35**, L03103
- De La Haye, V., et al. 2007, *J. Geophys. Res.*, **112**, A07309
- Dialynas, K., Krimigis, S., Mitchell, D. G., Hamilton, D. C., Krupp, N., & Brandt, P. C. 2008, *J. Geophys. Res.*, **114**, A01212
- Ezell, R. L., Edwards, A. K., & Wood, R. M. J. 1984, *Chem. Phys.*, **81**, 1341
- Flesch, G. D., et al. 1990, *J. Chem. Phys.*, **92**, 3235
- Garnier, P., et al. 2007, *Planet. Space Sci.*, **55**, 165
- Hartle, R. E., et al. 2006, *Planet. Space Sci.*, **54**, 1211
- Johnson, R. E. 1990, *Energetic Charged Particle Interactions with Atmospheres and Surfaces* (Berlin: Springer)
- Johnson, R. E. 1994, *Space Sci. Rev.*, **69**, 215
- Johnson, R. E. 2009, *Phil. Trans. R. Soc. A*, **367**, 753
- Johnson, R. E., Fama, M., Liu, M., Baragiola, R. A., Sittler, E. C., Jr., & Smith, H. T. 2008a, *Planet. Space Sci.*, **56**, 1238
- Johnson, R. E., Liu, M., & Sittler, E. C. 2005, *Geophys. Res. Lett.*, **32**, L24201
- Johnson, R. E., Smith, H. T., Tucker, O. J., Liu, M., & Tokar, R. 2006a, *ApJ*, **644**, L137
- Johnson, R. E., et al. 2006b, *Icarus*, **180**, 393
- Johnson, R. E., et al. 2008b, *Space Sci. Rev.*, **139**, 355
- Johnson, R. E., et al. 2009, *Mass Loss Processes at Titan in Titan after Cassini/Huygens* (Tucson, AZ: Univ. Arizona Press), in press
- Lafosse, A., Houver, J. C., & Doweck, D. 2001, *J. Phys. B: At. Mol. Opt. Phys.*, **34**, 819
- Ledvina, S. A., Cravens, T. E., & Keckskemety, K. 2005, *J. Geophys. Res.*, **110**, A06211
- Li, X., et al. 1997, *J. Chem. Phys.*, **106**, 1373
- Lindsay, B. G., et al. 1998, *Phys. Rev. A*, **57**, 331
- Luna, H., Michael, M., Shah, M. B., Johnson, R. E., Latimer, C. J., & McConkey, J. W. 2003, *J. Geophys. Res.*, **108**, 5033
- Luna, H., McGrath, C., Shah, M. B., Johnson, R. E., Liu, M., Latimer, C. J., & Montenegro, E. C. 2005, *ApJ*, **628**, 1086
- Lundqvist, M., Edvardsson, D., Baltzer, P., & Wannberg, B. 1996, *J. Phys. B: At. Mol. Opt. Phys.*, **29**, 1489
- Ma, Y., et al. 2006, *J. Geophys. Res.*, **111**, A05207
- Magee, B. A., Waite, J. H., Mandt, K. E., Westlake, J., Bell, J., & Gell, D. A. 2009, *Planet. Space Sci.*, in press
- McCartney, P. C. E., McGrath, C., McConkey, J. W., Shah, M. B., & Geddes, J. 1999, *J. Phys. B: At. Mol. Opt. Phys.*, **32**, 5103
- McGrath, C., Shah, M. B., McCartney, P. C. E., & McConkey, J. W. 2001, *Phys. Rev. A*, **64**, 062712
- Michael, M., & Johnson, R. E. 2005, *Planet. Space Sci.*, **53**, 1510
- Michael, M., Johnson, R. E., Leblanc, F., Liu, M., Luhmann, J. G., & Schematovich, V. I. 2005, *Icarus*, **175**, 263
- Nicolas, C., Alcaraz, C., Thissen, R., Vervloet, M., & Dutuit, O. 2003, *J. Phys. B: At. Mol. Opt. Phys.*, **36**, 2239
- Niemann, H. B., et al. 2005, *Nature*, **438**, 779
- Rymer, A. M., Smith, H. T., Wellbrock, A., Coates, A. J., & Young, D. T. 2009, *J. Geophys. Res.*, **36**, L15109
- Schematovich, V. I., Johnson, R. E., Michael, M., & Luhmann, J. G. 2003, *J. Geophys. Res.*, **108**, 5087
- Siegmann, B., Werner, U., Mann, R., Kabachnik, N. M., & Lutz, H. O. 2000, *Phys. Rev. A*, **62**, 022718
- Sillanpaa, I., Kallio, E., Janhunen, P., Schmidt, W., Mursula, K., Vilppola, J., & Tanskanen, P. 2006, *Adv. Space Res.*, **38**, 799
- Sillanpaa, I., Kallio, E., Jarvinen, R., & Janhunen, P. 2007, *J. Geophys. Res.*, **112**, A12205
- Sittler, E. C., et al. 2009, *Planet. Space Sci.*, in press
- Smith, H. T., Mitchell, D. G., Johnson, R. E., & Paranicas, C. P. 2009, *Planet. Space Sci.*, in press
- Stebbins, R. F., Turner, B. R., & Smith, A. C. H. 1963, *J. Chem. Phys.*, **38**, 2277
- Stier, P. M., & Barnett, C. F. 1956, *Phys. Rev.*, **103**, 896
- Wahlund, J.-E., et al. 2005, *Ionos. Titan Sci.*, **308**, 982
- Young, D. T., et al. 2005, *Science*, **307**, 1262
- Yousif, F. B., Lindsay, B. G., & Latimer, C. J. 1990, *J. Phys. B: At. Mol. Opt. Phys.*, **21**, 4157
- Ziegler, J. F., Biersack, J. P., & Littmark, U. 1985, *The Stopping and Ranges of Ions in Solids* (New York: Pergamon)